Eur. Phys. J. C 7, 73–86 (1999)
DOI 10.1007/s100529800986

THE EUROPEAN
PHYSICAL JOURNAL C

Diffractive photo- and leptoproduction of vector mesons ρ, ρ' and ρ''*

G. Kulzinger, H.G. Dosch, H.J. Pirner

Institut für Theoretische Physik der Universität Heidelberg, Philosophenweg 16 & 19, D-69120 Heidelberg, Germany
(e-mail: G.Kulzinger@thphys.uni-heidelberg.de)

Received: 16 June 1998 / Published online: 22 October 1998

Abstract. We calculate diffractive photo- and leptoproduction of ρ-, ρ'- and ρ''-mesons. The incoming photon dissociates into a $q\bar{q}$-dipole which scatters on the nucleon and transforms into a vector meson state. The scattering amplitude is calculated in non-perturbative QCD with the model of the stochastic vacuum. Assuming that the physical ρ'- and ρ''-mesons are mixed states of an active 2S-excitation and some residual hybrid state which cannot be produced diffractively in lowest order QCD, we obtain good agreement with the data, especially the markedly different spectrum in the $\pi^+\pi^-$-invariant mass for photoproduction and e^+e^--annihilation.

1 Introduction

Exclusive vector meson production by real and virtual photons is an efficient probe to investigate the physics of diffractive scattering. The experimental situation in $\pi^+\pi^-$- and $2\pi^+2\pi^-$-production in the mass range from 1–2 GeV is rather complex. Photoproduction data show one broad bump in the $\pi^+\pi^-$-mass distribution [1] on the upper tail of the ρ at around 1.6 GeV. The same enhancement is visible in $2\pi^+2\pi^-$-production [2]. In e^+e^--annihilation [3–5] a distinct interference pattern is seen. Evidence for two resonances has been established in Refs [6,7]. Both resonances couple with approximately equal strength to the electromagnetic current. Their masses are compatible with those of the 1^{--} states $\rho(1450)$ and $\rho(1700)$, respectively.

In [8] good agreement with experimental data for ρ-production at moderate and high photon virtualties Q^2 was obtained. This success, based on the specific model of the stochastic vacuum for non-perturbative QCD, sheds new light on the nature of the pomeron. Since the stochastic gluon field strength correlators in the vacuum explain confinement, their application to the physics of the pomeron builds an important bridge between low-energy non-perturbative physics and high-energy scattering at long distances. The coupling of the photon to the $q\bar{q}$-dipole is taken from perturbation theory. This approach has been checked in inclusive photon scattering at high Q^2 [9], where at fixed scattering energy W the same photon wave function and reaction mechanism reproduce the structure function F_2.

For low $Q^2 < 1\,\mathrm{GeV}^2$ the perturbative photon wave function is not acceptable, since the resulting large $q\bar{q}$-dipoles feel confinement and chiral symmetry breaking. A way out of this dilemma has been shown in [9], where a Q^2-dependent quark mass, determined from comparison with the phenomenological correlator of the vector current, has been introduced in the perturbative photon wave function. This effective mass mimics chiral symmetry breaking and also confinement in the Euclidean region as has been shown in a detailed model investigation of the harmonic oscillator. Comparison with the phenomenological correlator indicates that chiral symmetry is effectively restored at $Q^2 > 1\,\mathrm{GeV}^2$, the constituent quark goes over into a partonic massless quark. Such a transition with resolution Q^2 is also seen in theoretical renormalization flow equations [10,11]. It is intimately connected with the chiral phase transition at finite temperatures. The calculation of diffractive vector meson production at low Q^2 in the following paper will present an additional test of the validity for the chiral transition.

Vector dominance or generalized vector dominance could be in principle another approach to treat the low-Q^2 virtual photon. We found, however, that the method has little predictive power since the results depend very strongly on couplings of the inserted vector meson states to the vector current; also the number of inserted vector meson states influences the results crucially. This behaviour is not unexpected, because the construction of a transverse wave function of a virtual photon, composed of wave functions of excited vector mesons, has to imitate a delicate cancellation at large distances. A similar feature can be seen very clearly in the harmonic oscillator model. In our opinion the modified perturbative $q\bar{q}$-wave function of the photon is a more reliable and more predictive de-

* Supported by the Deutsche Forschungsgemeinschaft under grant no. GRK 216/1-96, by the EU grant FMRX-CT96-0008 and by the Federal Ministry of Education, Science, Research and Technology (BMBF), grant no. 06 HD 855

scription of the low-Q^2 physics than the treatment with generalized vector dominance.

The outline of the paper is as follows: In Sect. 2 we give the light-cone wave functions of the ρ, ρ' and ρ''. Section 2 also contains our comparison of theory with experimental branching ratios and decay widths. In Sect. 3 we calculate the matrix elements and cross sections for diffractive production of the vector meson states by real and virtual photons. Section 4 concludes with a discussion and summary.

2 Wave functions and properties of ρ, ρ' and ρ''

2.1 Light-cone wave functions

The hadronic light-cone wave functions of the mesons represent an important input to exclusive scattering. In the perturbative regime for longitudinal photons at high Q^2 the wave function at the origin dominates the production process. This value of the wave function is known from the measured e^+e^--width. Parametrizations of the ground state vector mesons based on this empirical information have been developed in [8]. Here we want to extend this work to the excited light vector mesons ρ' and ρ''. An analysis of the experimental data from e^+e^--annihilation and photoproduction of (π^+,π^-) shows that there are at least two excited ρ-resonances, the $\rho(1450)$ and the $\rho(1700)$ [6]. Recently [7,12] it has been speculated that there may be a hybrid state $h(1450)$ with the quantum numbers of the ρ-meson which decays predominantly into πa_1.

The genuine quark model states are the $2S$- and $2D$-excitations. The $2S$-state couples to the photon strongly, whereas the $2D$-state has a vanishing wave function at the origin and consequently only a small relativistically induced coupling to the photon [13]. Also diffraction proceeds mostly without angular momentum transfer, so the production of the $2D$-state is suppressed. In the following we will use a simplified ansatz for the vector meson states. We employ the nonrelativistic notation $1S$ and $2S$ as a short hand notation for light-cone wave functions which in the nonrelativistic limit have this character. Our ansatz for the physical vector meson states has the following form:

$$\begin{aligned} |\rho(770)\rangle &= |1S\rangle\,, \\ |\rho(1450)\rangle &= \cos\theta\,|2S\rangle + \sin\theta\,|rest\rangle\,, \\ |\rho(1700)\rangle &= -\sin\theta\,|2S\rangle + \cos\theta\,|rest\rangle\,. \end{aligned} \tag{1}$$

Here the state $|rest\rangle$ describes the $|2D\rangle$- and hybrid $|h\rangle$-states whose coupling to the photon are suppressed and which hence we neglect in our approach. For details of the wave functions both for the photon and the vector mesons we refer to Appendix B.

2.1.1 Photon wave function

For the photon wave function we use the form derived in [8] with a running quark mass $m(Q^2)$ in order to take into account chiral symmetry breaking and confinement at large distances in an approximate way. It depends on the light-cone momentum fraction z of the quark and the transverse distance r between the quark and the antiquark. The index λ indicates the helicity of the photon, h and $\bar{h}$ give the quark and antiquark helicities:

$$\psi_{\gamma(Q^2,\lambda)}(z,\mathbf{r}) = \sqrt{N_c}\; e_f\; \delta_{f\bar{f}}\; \chi_{\gamma(Q^2,\lambda)}(z,\mathbf{r})\,, \tag{2}$$

with[1]

$$\chi_{\gamma(Q^2,\lambda=0)} = -\delta_{h,-\bar{h}}\; 2z(1-z)\; Q\; \frac{K_0(\varepsilon r)}{2\pi}\,, \tag{3}$$

$$\begin{aligned} \chi_{\gamma(Q^2,\lambda=+1)} = \sqrt{2}\Big\{ & i\mathrm{e}^{i\varphi}\;\varepsilon\left(z\delta_{h+,\bar{h}-} - (1-z)\delta_{h-,\bar{h}+}\right) \\ & \times\frac{K_1(\varepsilon r)}{2\pi} + m(Q^2)\,\delta_{h+,\bar{h}+}\,\frac{K_0(\varepsilon r)}{2\pi}\Big\}\,, \end{aligned}$$

$$\begin{aligned} \chi_{\gamma(Q^2,\lambda=-1)} = \sqrt{2}\Big\{ & i\mathrm{e}^{-i\varphi}\varepsilon\left((1-z)\delta_{h+,\bar{h}-} - z\delta_{h-,\bar{h}+}\right) \\ & \times\frac{K_1(\varepsilon r)}{2\pi} + m(Q^2)\,\delta_{h-,\bar{h}-}\,\frac{K_0(\varepsilon r)}{2\pi}\Big\}\,, \end{aligned}$$

where φ is the azimut angle and

$$\varepsilon = \sqrt{z(1-z)Q^2 + m^2(Q^2)}\,. \tag{4}$$

The running quark mass was determined to evolve as

$$m(Q^2) = \begin{cases} 0.220\ \mathrm{GeV}\cdot\left(1 - Q^2/Q_0^2\right), & Q^2 < Q_0^2 = 1.05\ \mathrm{GeV}^2\,, \\ 0, & Q^2 \geq Q_0^2\,, \end{cases} \tag{5}$$

in [9] by matching the vector current correlator.

2.1.2 Vector meson wave functions

The vector meson light-cone wave functions are parametrized in an analogous way. One has to rely on such a phenomenological construction as long as not even the form of the light-cone Hamiltonian for valence states is known. However, there are attempts to construct light-cone wave functions via a Melosh transformation from solutions of a relativized constituent quark model Hamiltonian [14]. Recently, also a string equation for the meson on the light-cone has been solved [15]. Since both approaches have not specified the solutions for the vector states in a parametrized form, we use model wave functions similar to those of Wirbel and Stech [16] to set up the wave functions for the quark-antiquark $1S$- and $2S$-excitations. Since the contributions of z near the endpoints are not significant for production of vector mesons at moderate Q^2 the argument against factorization of [17] and [18] have here no practical consequence, see also [19].

[1] In the following some indices and arguments are not given explicitely in order not to overload the notation

For convenience we introduce the following abbreviations:

$$h_{V,\lambda}(z) = \mathcal{N}_{V,\lambda}\ \sqrt{z(1-z)} \times \exp\left\{-\frac{1}{2}\,\frac{M^2(z-1/2)^2}{\omega_{V,\lambda}^2}\right\}\ , \quad (6)$$

$$g_{V,\lambda}(r) = \exp\left\{-\frac{1}{2}\,\omega_{V,\lambda}^2\, r^2\right\}\ , \quad (7)$$

where $\lambda = L, T$ refers to longitudinal and transverse polarization and $V = 1, 2$ to the $1S$- and $2S$-state; M is the mass of the $1S$-state, i.e. of the ρ-meson. We have the following wave functions:

$1S$, longitudinal:

$$\psi_{1(L)} = \delta_{h,-\bar{h}}\ 4z(1-z)\ \omega_{1L}\ h_{1L}(z)\, g_{1L}(r)\ . \quad (8)$$

$1S$, transverse:

$$\psi_{1(\lambda=+1)} = h_{1T}(z)\, g_{1T}(r)\left\{i\omega_{1T}^2 r \mathrm{e}^{i\varphi}\left(z\delta_{h,+}\delta_{\bar{h},-} -(1-z)\delta_{h,-}\delta_{\bar{h},+}\right) + m(Q^2)\,\delta_{h,+}\delta_{\bar{h},+}\right\}\ ,$$
$$\psi_{1(\lambda=-1)} = h_{1T}(z)\, g_{1T}(r)\left\{i\omega_{1T}^2 r \mathrm{e}^{-i\varphi}\left((1-z)\delta_{h,+}\delta_{\bar{h},-} -z\delta_{h,-}\,\delta_{\bar{h},+}\right) + m(Q^2)\,\delta_{h,-}\,\delta_{\bar{h},-}\right\}\ . \quad (9)$$

For the $2S$-state we allow for an excitation in the transverse plane by taking in momentum space the excited two dimensional harmonic oscillator wave function, for the excitation in the 3-direction we introduce a polynomial quadratic in z and symmetric under interchange of z and $(1-z)$. It is further fixed by the condition that the $2S$-state is orthogonal on the $1S$-state. We thus obtain:

$2S$, longitudinal:

$$\psi_{2(L)} = \delta_{h,-\bar{h}} 4z(1-z)\omega_{2L} h_{2L}(z)\, g_{2L}(r) \times\left\{(z(1-z)-A_L) + \sqrt{2}(\omega_{2L}^2 r^2 - 1)\right\}\ . \quad (10)$$

$2S$, transverse:

$$\psi_{2(\lambda=+1)} = h_{2T}(z)\, g_{2T}(r)\Big\{i\omega_{2T}^2 r \mathrm{e}^{i\varphi}\left(z\delta_{h,+}\,\delta_{\bar{h},-} -(1-z)\delta_{h,-}\delta_{\bar{h},+}\right)\Big[(z(1-z)-A_T) +\sqrt{2}\,(\omega_{2T}^2 r^2 - 3)\Big] + m(Q^2)\,\delta_{h,+}\,\delta_{\bar{h},+} \times\Big[(z(1-z)-A_T) + \sqrt{2}\,(\omega_{2T}^2 r^2 - 1)\Big]\Big\}\ ,$$
$$\psi_{2(\lambda=-1)} = h_{2T}(z)\, g_{2T}(r)\Big\{i\omega_{2T}^2 r \mathrm{e}^{-i\varphi}\left((1-z)\delta_{h,+}\,\delta_{\bar{h},-} -z\delta_{h,-}\,\delta_{\bar{h},+}\right)\Big[(z(1-z)-A_T) +\sqrt{2}\,(\omega_{2T}^2 r^2 - 3)\Big] + m(Q^2)\,\delta_{h,-}\,\delta_{\bar{h},-} \times\Big[(z(1-z)-A_T) + \sqrt{2}\,(\omega_{2T}^2 r^2 - 1)\Big]\Big\}; \quad (11)$$

the factor $\sqrt{2}$ accounts for the two transverse excitation modes.

Table 1. The parameters for the $1S$- and $2S$-wave functions. Besides the ρ-mass the bold face quantities are input. The values $\omega_{2\lambda}$ are adjusted in order to have agreement of f_{2L} with f_{2T}

State	$f_{V,\lambda}$[GeV]	$\omega_{V,\lambda}$[GeV]	$\mathcal{N}_{V,\lambda}$	A_λ
$1S$-Longitudinal	**0.1526**	0.330	4.48	
$1S$-Transverse	**0.1526**	0.213	3.44	
$2S$-Longitudinal	−0.137	**0.297**	3.21	0.228
$2S$-Transverse	−0.137	**0.235**	1.96	−0.328

The normalization constants $\mathcal{N}_{1\lambda}$ are fixed by the wave function normalization. The oscillator frequencies $\omega_{1\lambda}$ are chosen in such a way as to reproduce the ρ-meson electromagnetic decay coupling $f_{1L} = f_{1T}$. The values for $\omega_{2\lambda}$ were minimally deviated from the $1S$-values in order to give the same $2S$-leptonic coupling for the longitudinal and transverse state. The constants $\mathcal{N}_{2\lambda}$ and A_L, A_T are determined by the requirement that the $2S$-state is both normalized and orthogonal on the $1S$-state. For details we refer to Appendix B. In Table 1 we collect the relevant parameters.

2.2 Properties of the physical ρ-, ρ'- and ρ''-states

The mixing angle θ is determined by fitting the experimental branching ratios

$$X_1 = B_{e^+e^-}\, B_{\pi^+\pi^-}\ , \quad (12)$$
$$X_2 = B_{2\pi^+2\pi^-}/B_{\pi^+\pi^-}\ ,$$
$$X_3 = B_{\pi^+\pi^-} + B_{2\pi^+2\pi^-}$$

for the ρ'- and ρ''-resonances; it is calculated in Appendix C:

$$\theta = 41.2^\circ\ . \quad (13)$$

In Table 2 we summarize the main properties of the three physical states ρ, ρ' and ρ''. There is considerable uncertainty about the magnitude of $\Gamma_{V\to e^+e^-}$ for the resonances ρ' and ρ''. The theoretical dilepton spectrum is in fair agreement with the data, cf. Fig. 1. In the 1.6 GeV region a destructive interference pattern shows up which fixes the relative signs of the vector meson couplings f_V as $(+,-,+)$. The signs of the decay constants of the ρ' and ρ'' correspond to the negative sign of the $2S$-wave function at the origin, cf. (10) and (11), and the mixing angle $\theta = 41.2^\circ$ in the first quadrant. In the same way as the dilepton width, e^+e^--annihilation measures the short range part of the wave functions; therefore the couplings f_V essentially determine both (see Appendix A). At first sight the opposite pattern with a constructive interference in photoproduction is puzzling, see Fig. 2.

Because of the decay into πa_1 the ρ'- and ρ''-resonances are considered as candidates for hybrid states in [12]. On

Table 2. Properties of the ρ-, ρ'- and ρ''-states. The couplings of ρ' and ρ'' to the electromagnetic current (bold face) result from both the physical states taken as mixed states according to (1) and the state $|2S\rangle$ being normalized and orthogonal on $|1S\rangle$. For the masses, total and ρ-meson electromagnetic decay width see [30]. The values X_1 and X_2 (see (12)) for ρ' and ρ'' are taken from an analysis by Donnachie and Mirzaie [6] of the (π^+, π^-)-mass spectra in photoproduction and e^+e^--annihilation. Within the given accuracy we set $B_{\rho\to\pi^+\pi^-} = 1$ and estimate the branching ratios of ρ' and ρ'' in two or four charged pions to 80%. The last two lines summarize the branching ratios

	ρ	ρ'	ρ''
M_V[GeV]	0.7681 ± 0.0013	1.465 ± 0.025	1.700 ± 0.020
Γ_V^{tot}[GeV]	0.1509 ± 0.0030	0.310 ± 0.060	0.235 ± 0.050
$\Gamma_{V\to e^+e^-}$[GeV]	$(6.77 \pm 0.32)\times 10^{-6}$	$\mathbf{1.63\times 10^{-6}}$	$\mathbf{1.07\times 10^{-6}}$
f_V[GeV]	0.1526	$\mathbf{-0.103}$	$\mathbf{+0.0903}$
X_1	4.48×10^{-5}	5.2×10^{-7}	6×10^{-7}
X_2	0	12.5	9.17
X_3	1	0.8	0.8
$B_{V\to\pi^+\pi^-}$	1	0.0593	0.0787
$B_{V\to 2\pi^+ 2\pi^-}$	0	0.741	0.721

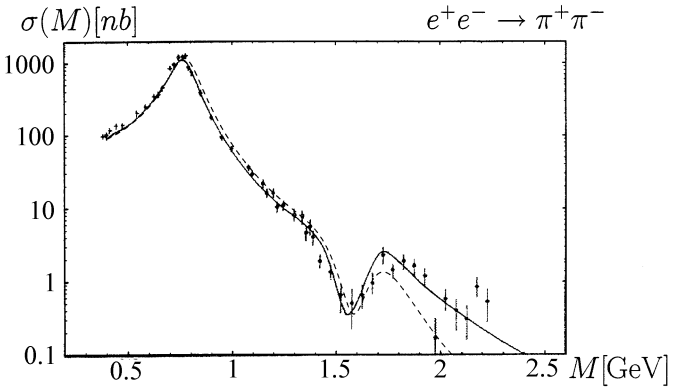

Fig. 1. Mass spectrum of e^+e^--annihilation into $\pi^+\pi^-$. In the 1.6 GeV region a destructive interference shows up determining the sign pattern $(+,-,+)$ of the vector meson couplings f_V to the electromagnetic current. The full curve is the fit of Donnachie and Mirzaie [6]. The dashed line is the parametrization for ρ' and ρ'' used in this paper (see Table 2 and Appendix A)

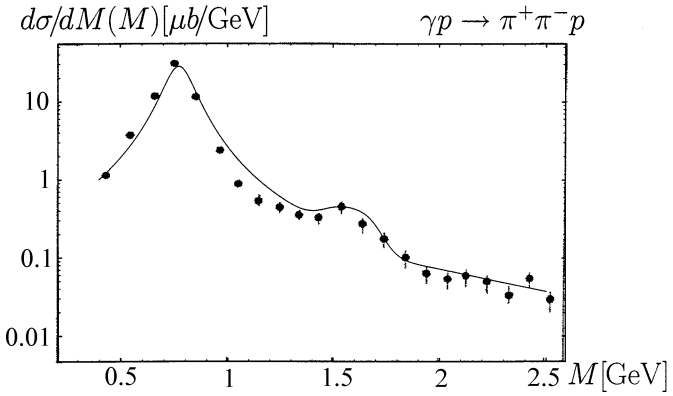

Fig. 2. Mass spectrum of $\pi^+\pi^-$-photoproduction on the proton. The interference in the 1.6 GeV region is constructive. The solid line is our result for $\pi^+\pi^-$-photoproduction using simple Breit-Wigner distributions for the ρ, ρ' and ρ''. Experimental points are not normalized and taken from Aston et al. [1], with a contribution of 50 ± 20 nb from the $g(1690)$ subtracted [29] (see also [6]

the other hand the presence of an $\omega\pi$-decay channel calls for a $2S$-component. For the ρ'' the analysis of the decay channels does not demand a mixing, but allows the presence of a hybrid component in the wave function.

3 Diffractive cross sections

The diffractive matrix elements for vector meson production are evaluated in the specific model of the stochastic vacuum (MSV), see Refs [8,9,20]. One feature of this model is that the same mechanism which confines quarks also induces a string-string interaction of colour singlet states which leads to a cross section increasing with the $q\bar{q}$-dipole size roughly like $r^{1.5}$, when r is in the interesting range of 1 fm $< r <$ 2 fm. In an alternative model of dipole-proton scattering, cf. Refs [21,22], there is a non-perturbative dipole-proton cross section which amounts to about half of the total value for $0 \le r \le 2$ fm. The other half of the cross section comes from a perturbative two-gluon exchange which saturates at $r = 1$ fm. The difference between the two descriptions is most pronounced at distances 1 fm $\le r \le 2$ fm. Such large dipole sizes can only be tested with excited meson states like the ρ-resonances. It is decisive to investigate the photo- and leptoproduction of ρ'- and ρ''-mesons. These experiments hold the key to find important long-range gluon fluctuations in diffraction which are related to confinement in low-energy spectroscopy.

The T-scattering amplitude is given by the integral over z and r of the wave function overlap summed over

quark helicities and multiplied with the dipole-proton amplitude:

$$T_V^\lambda(s,t) = is \int \frac{dz d^2\mathbf{r}}{4\pi}\, \psi^\dagger_{V(\lambda)}\psi_{\gamma(Q^2,\lambda)}(z,\mathbf{r})\, J_p(z,\mathbf{r},\Delta_T)\ , \tag{14}$$

where the invariant momentum transfer squared $t = -\Delta_T^2$ (up to corrections of the order s^{-2}, cf. [8]) and the amplitude J_p has the form:

$$J_p(z,\mathbf{r},\Delta_T) = 2\int_0^\infty bdb\, 2\pi J_0(\Delta_T b) \times \int \frac{dz_p d^2\mathbf{r}_p}{4\pi}\, |\psi_p(z_p,\mathbf{r}_p)|^2 J(b,z,\mathbf{r},z_p,\mathbf{r}_p)\ . \tag{15}$$

The kernel $J(b,z,\mathbf{r},z_p,\mathbf{r}_p)$ is provided by the MSV and can be understood as the interaction amplitude for the scattering of two colour dipoles, where the second, with index "p", denotes a proton in the quark-diquark picture; b is the scattering impact parameter. This kernel as well as the profile function $J_p(z,\mathbf{r},\Delta_T)$ are the same as in previous work on moderate- and high-Q^2 vector meson production. The Bessel function J_0 is obtained from the angular integral in the Fourier transform. For a detailed discussion see [8].

With (14) as definition of the T-amplitude the differential cross section with respect to t writes

$$\frac{d\sigma_V^\lambda}{dt}(t) = \frac{1}{16\pi s^2}\,|T_V^\lambda(s,t)|^2\ . \tag{16}$$

Note, that the MSV evaluates J_p in an eikonal approximation which causes the T-amplitude to depend on s only kinematically. Integration over t yield cross sections σ_V^λ which are constant and refer to a scattering energy $\sqrt{s} = 20$ GeV where the parameters of the model are fixed (see discussion below). For unpolarized photons the experimental data include transverse and longitudinal contribution:

$$\sigma = \sigma^T + \epsilon\sigma^L\ , \tag{17}$$

where the rate ϵ of longitudinally polarized photons depends on the lepton scattering angle, the photon energy and virtuality and typically varies in the range from 0.7 to 1, see Table 3 and [8].

In Fig. 3 we display the quantity

$$J_p^{(0)}(z,r) := \int_0^{2\pi} \frac{d\varphi_{\mathbf{r}}}{2\pi}\, J_p(z,\mathbf{r},\Delta_T = 0) \tag{18}$$

Due to the optical theorem it describes the total cross section of a dipole with light-cone fraction z and size r (averaged over all its orientations) on a proton. It depends only very slightly on z and we display it for the central value $z = 1/2$. The grey lines show the contribution of a completely abelian model (which cannot yield confinement), whereas the full lines represent the dipole-proton cross section as evaluated in the MSV. The monotonous rise at large values of r is a consequence of a string-string interaction [8,20]. It depends crucially on the field strengths correlators. The input parameters have been fixed in order to obtain a consistent picture of the slope of the $q\bar{q}$-confining potential, the numerical results for the correlators from lattice simulations and proton-proton scattering at a scattering energy $\sqrt{s} = 20$ GeV, where hadron-hadron cross sections are approximately energy independent. All absolute cross sections calculated in the following refer thus to this energy. For ratios of cross sections our results are also relevant at higher energies, since change with $\sqrt{s}$ should affect numerator and denominator approximately in the same way.

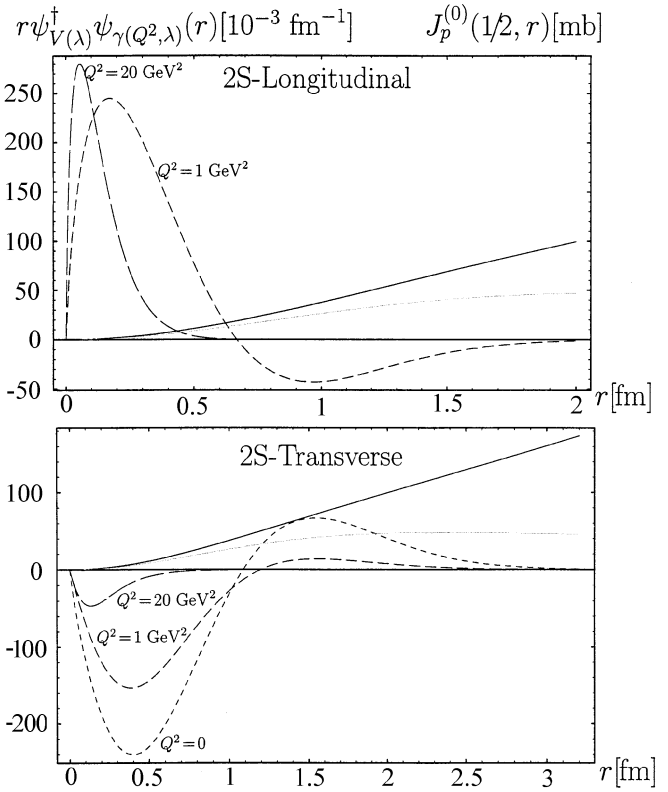

Fig. 3. Dipole-proton total cross section $J_p^{(0)}$ and the effective overlap $r\psi^\dagger_{V(\lambda)}\psi_{\gamma(Q^2,\lambda)}$ as function of the transverse dipole size r. The black lines are the function $J_p^{(0)}(z=1/2,r)$ (18), i.e. the total cross section of a dipole of fixed light-cone fraction $z = 1/2$ and transverse extension r, averaged over all orientations, as a function of r; the grey lines show the cross section of a completely abelian, non-confining theory. The leptoproduction amplitude is obtained by integration over the product of J_p and the overlap function, which essentially (cf. (19)) is the quantity shown for $Q^2 = 0$, 1 and 20 GeV^2 as short, medium and long dashed curves, respectively

The second important input to the diffractive leptoproduction cross section are the overlap matrix elements of the incoming photon with the outgoing vector meson. As has already been pointed out in [22] the node in the $2S$-state leads to a compensation of contributions of large and small dipole sizes. For our investigation this compensation is particularly interesting since it allows very specific tests

Table 3. Theoretical cross sections for ρ-meson photo- and leptoproduction in comparison with data from NMC [23] and E665 [24], the latter with separate transverse and longitudinal polarizations. The experimental data contain a Regge contribution which at these energies can be estimated to about 15%

Integrated ρ-cross sections: theory vs experiment							
Q^2 [GeV^2]	σ^T [μb]		σ^L [μb]		ϵ	$\sigma^T+\epsilon\sigma^L$ [μb]	
	th.[a]	exp.	th.[a]	exp.	exp.	th.[a]	exp.
0	7.86	9.4±1.1 [b]					
0.17	4.28	6.37±0.89	0.517	1.39±0.26	0.76	4.67	7.42±0.91
0.25	3.37	4.11±0.23	0.603	1.15±0.12	0.80	3.85	5.03±0.25
0.43	2.14	2.67±0.13	0.645	1.051±0.081	0.81	2.66	3.52±0.15
0.76	1.12	1.269±0.073	0.530	0.708±0.052	0.81	1.55	1.84±0.084
1.35	0.426	0.533±0.045	0.300	0.422±0.040	0.81	0.669	0.875±0.055
2.39	0.127	0.165±0.022	0.135	0.185±0.025	0.81	0.237	0.315±0.030
2.5	$115.\times10^{-3}$	—	$126.\times10^{-3}$	—	0.50	$178.\times10^{-3}$	$(170\pm31)\times10^{-3}$
3.5	51.6×10^{-3}	—	71.7×10^{-3}	—	0.66	98.9×10^{-3}	$(60\pm10)\times10^{-3}$
4.23	32.0×10^{-3}	$(55\pm11)\times10^{-3}$	50.7×10^{-3}	$(88\pm17)\times10^{-3}$	0.81	73.1×10^{-3}	$(126\pm18)\times10^{-3}$
4.5	27.3×10^{-3}	—	45.1×10^{-3}	—	0.66	57.1×10^{-3}	$(65\pm11)\times10^{-3}$
5.5	16.1×10^{-3}	—	30.4×10^{-3}	—	0.72	38.0×10^{-3}	$(41\pm7)\times10^{-3}$
6.9	8.68×10^{-3}	—	19.0×10^{-3}	—	0.76	23.1×10^{-3}	$(23\pm3)\times10^{-3}$
7.51	6.85×10^{-3}	$(17\pm5)\times10^{-3}$	15.8×10^{-3}	$(38\pm11)\times10^{-3}$	0.81	19.7×10^{-3}	$(47.8\pm10.2)\times10^{-3}$
8.8	4.36×10^{-3}	—	11.1×10^{-3}	—	0.78	13.1×10^{-3}	$(15\pm2)\times10^{-3}$
11.9	1.80×10^{-3}	—	5.55×10^{-3}	—	0.82	6.35×10^{-3}	$(5.8\pm0.9)\times10^{-3}$
16.9	0.617×10^{-3}	—	2.36×10^{-3}	—	0.81	2.53×10^{-3}	$(2.6\pm0.7)\times10^{-3}$

[a] Pomeron contribution

[b] For photon energies $20<\nu<70$ GeV, Ref. [2].

of the dipole cross section at large distances where the MSV makes specific predictions. In order to exhibit this effect we display in Fig. 3 the overlap function which is for demonstration purpose integrated over z and averaged over all orientations

$$r\psi^\dagger_{V(\lambda)}\psi_{\gamma(Q^2,\lambda)}(r) := \int \frac{dz}{4\pi} \int_0^{2\pi} \frac{d\varphi_{\mathbf{r}}}{2\pi} \, |\mathbf{r}| \, \psi^\dagger_{V(\lambda)}\psi_{\gamma(Q^2,\lambda)}(z,\mathbf{r}) \, , \qquad (19)$$

both for transverse and longitudinal photons and several values of Q^2.

The T-amplitude $T_V^\lambda(s,t)$, cf. (14), can be estimated from Fig. 3 by multiplying the dipole-proton cross section with the overlap function and integrating over r.

The change of sign in the $2S$-wave function makes the T-amplitude very sensitive to the behaviour of the dipole-proton cross section $J_p(z,r,\Delta_T)$ at larger values of r. Only its strong increase can overcome the negative contribution below the node and lead to a positive sign of the imaginary part of $T_V^\lambda(s,t)$. This will turn out to be crucial for the explanation of the different interference patterns in photoproduction and e^+e^--annihilation mentioned in Sect. 2 and shown in Figs. 1 and 2.

The importance of the outer region, in particular for the $2S$-state, can also be seen from Fig. 4: There the cross section is calculated as function of an upper cut-off $r_{\rm cut}$ in the r-integration of (14). As can clearly be seen, in photoproduction the inner region of the overlap dominates for $r \lesssim 1.2$ fm, but compensation occurs at $r_{\rm cut} \cong 1.7$ fm from the outer region, which contributes significantly to the T-amplitude up to r-values of about 2.5 fm. By varying the photon-virtuality Q^2 one shifts the position of the node in the overlap and thus the weight of the negative and positive contributions. This is reflected in the strong Q^2-dependence of the $\sigma(r_{\rm cut})$-curves in Fig. 4 and the structured Q^2-dependence of the transverse and longitudinal cross sections in Fig. 5. For the transverse cross section the outer positive region dominates for $Q^2 \lesssim 0.3$ GeV^2, where there is a dip in the $2S$-transverse cross section; for the longitudinal one the dip is at $Q^2 \cong 2.5$ GeV^2. For high Q^2-values only small dipole sizes r contribute (early saturation in Fig. 4) since the vector meson wave function suppresses the endpoint values of the longitudinal momentum fraction z.

In order to trace the experimental behaviour of the cross section as function of the invariant mass M of the pions one needs the amplitudes of the ρ'- and ρ''-resonances separately.

Experimentally the $\pi^+\pi^-$- and $2\pi^+2\pi^-$-cross sections are measured. Here it is essential to include the relevant branching ratios and the finite widths of the resonances which in our case lead to a considerable reduction of the cross section as compared to a zero-width approach. In detail we calculate for the final states $f = \pi^+\pi^-$ and $2\pi^+2\pi^-$ the differential cross sections in respect to their invariant mass M:

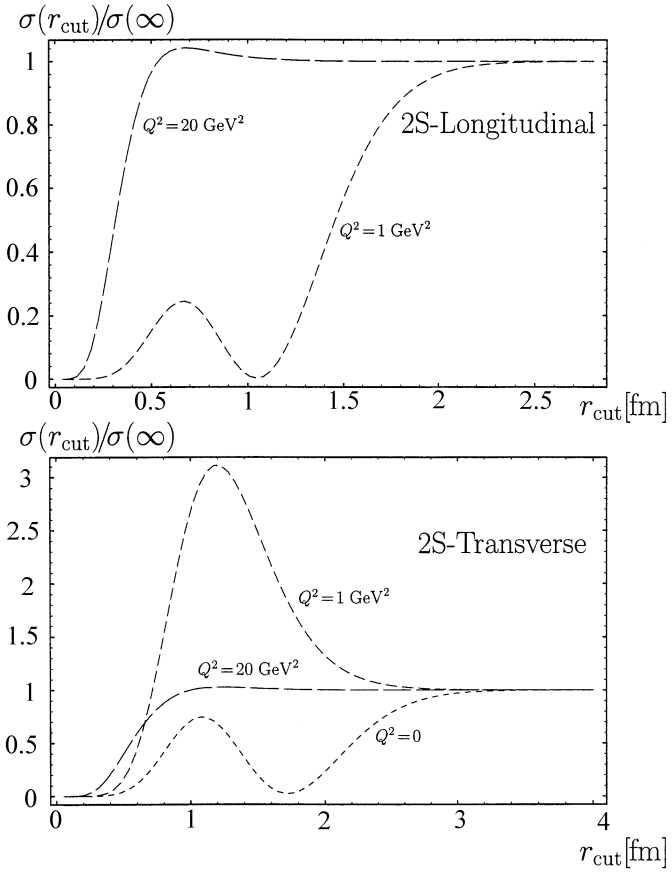

Fig. 4. Fraction of production cross sections due to dipole sizes smaller than $r_{\rm cut}$. The short, medium and long dashed curves refer to $Q^2 = 0,\ 1$ and 20 GeV^2, respectively. Due to the node in the wave function of the $2S$-state (see Fig. 3) the contribution of large dipole sizes is particularly important for small values of Q^2

$$\frac{d\sigma^{f,\lambda}}{dM} = \frac{2M}{16\pi s^2}\int dt \left| \sum_{V=\rho,\rho',\rho''} T_V^{\lambda}(s,t)\sqrt{\frac{M_V\Gamma_V^{tot}}{\pi}} \times \frac{c_{Vf}}{M^2 - M_V^2 + iM_V\Gamma_V^{tot}}\sqrt{B_{V\to f}}\right|^2 . \quad (20)$$

For the branching ratios $B_{V\to f}$ we refer to the discussion in Table 2; the c_{Vf} arise from proper normalization, cf. (A10) and (A11), and deviate from 1 on the few-percent-level.

In the upper part of Fig. 5 we show the transverse and longitudinal ρ-production cross section for values $0.02\ \text{GeV}^2 \le Q^2 \le 20\ \text{GeV}^2$ together with the data from NMC [23] and E665 [24]. The theoretical photoproduction cross section is $\sigma_{\gamma p} = 7.9\mu$b, the experimental value $9.4 \pm 1.1\mu$b [2]. The experimental data contains also Reggeon, i.e. non-diffractive exchange which we have not taken into account. We may roughly estimate the contribution at least for low Q^2 by compairing with the Donnachie-Landshoff parametrization [25] of the total γp-cross section. There at $\sqrt{s} = 20$ GeV the Reggeon contribution is 7 percent, hence we estimate for the production

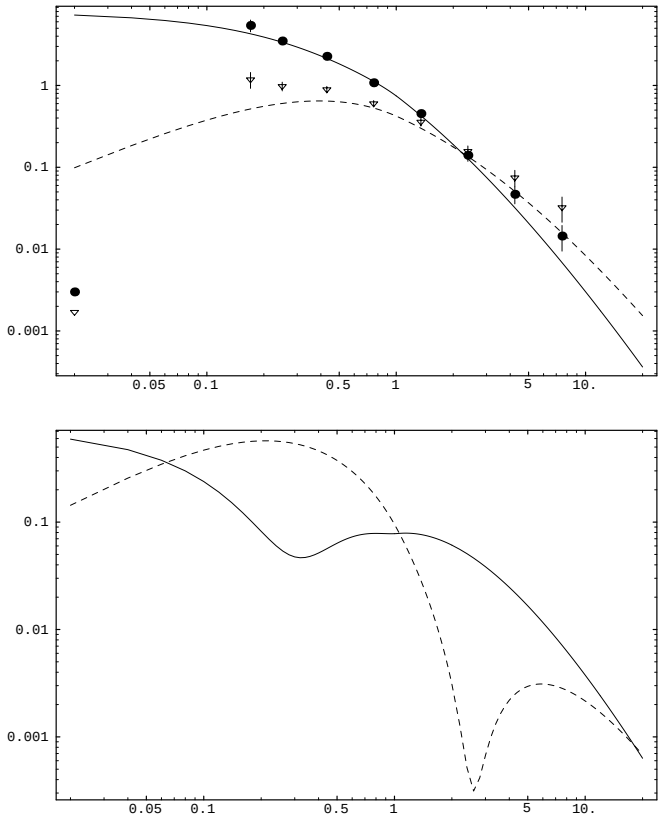

Fig. 5. Integrated elastic cross sections of the ρ-meson and the 2S-state as a function of the photon virtuality Q^2. E665 [24] provides data for the ρ, cf. Table 3; we roughly estimate the pomeron contribution as 85% of the measured cross section

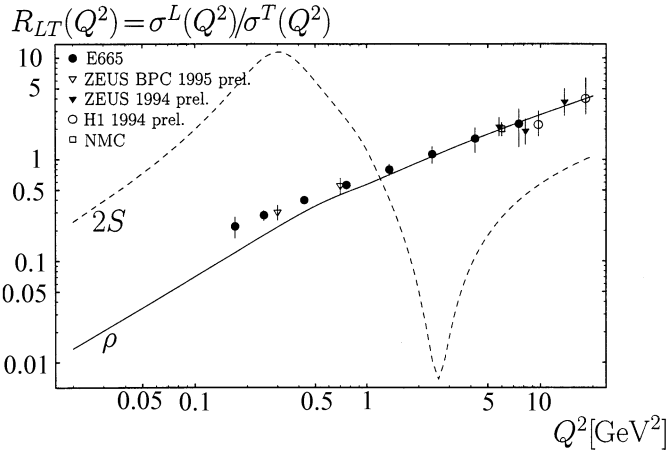

Fig. 6. Ratio of longitudinal over transverse integrated cross sections as function of Q^2 both for the ρ-meson (*full*) and the $2S$-state (*dashed*). There is only data for ρ-production

cross section, i.e. the square of the amplitude, a Reggeon contribution of 15 percent. As constituent quark mass we use $m(Q^2)$ as it has been determined from the vector current correlator and used in inclusive photoproduction, cf. [9]. At moderate Q^2 the E665 data are almost 20–30% higher than our theoretical calculations, but an extrapolation of the E665 data lies by about the same amount above the NMC data, which we reproduce quite well. At

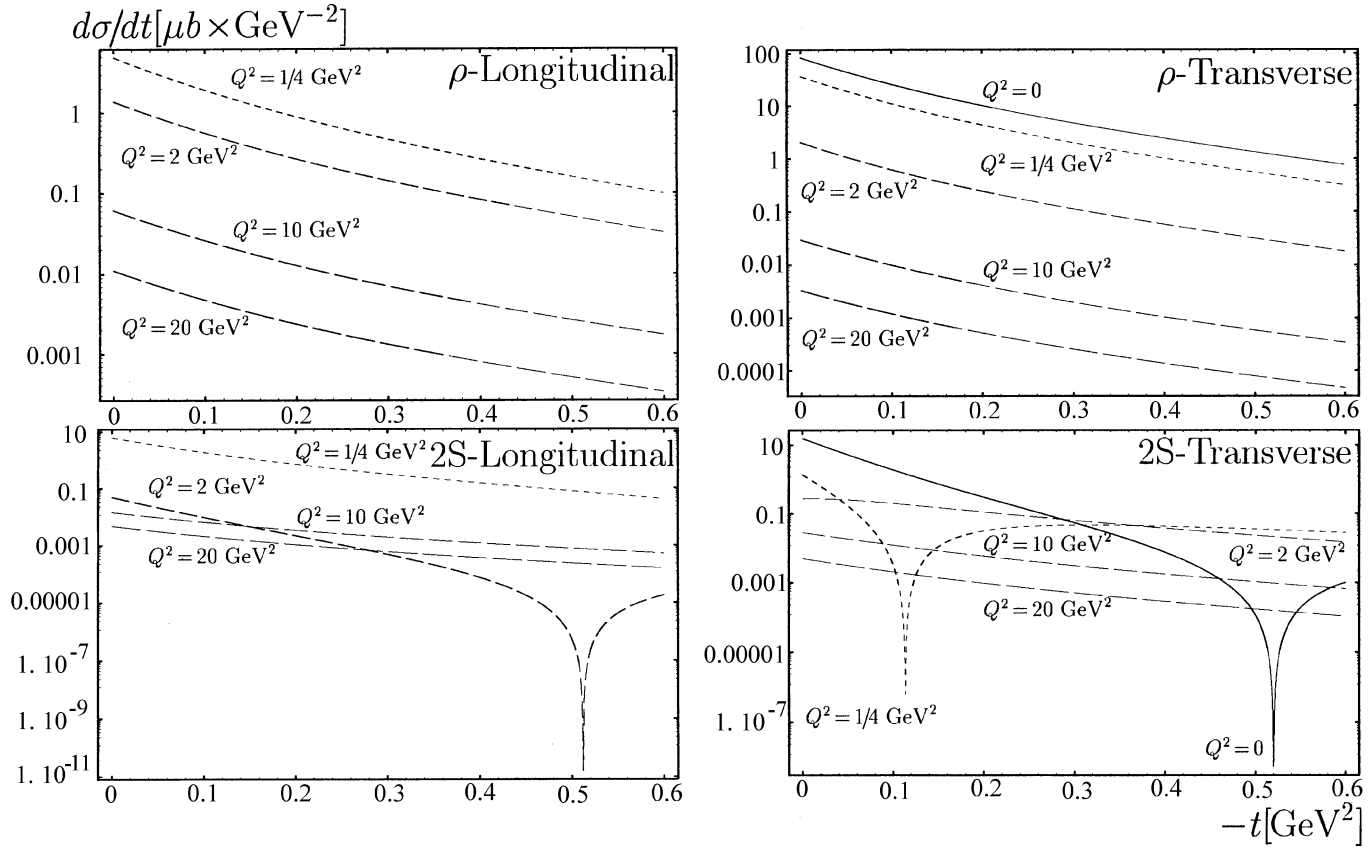

Fig. 7. Differential cross section as a function of $-t$ for the ρ-meson and the $2S$-state (upper and lower plots) for both longitudinal and transverse polarization (left and right). The curves with increasing dash sizes refer to $Q^2 = 0,\ 1/4,\ 2,\ 10,\ 20$ GeV. For the $2S$-state the node in the wave function has a strong influence on the t-dependence

$Q^2 > 1$ GeV^2 the theoretical cross sections are identical to the previously calculated $\gamma p \to \rho p$ cross sections, see [8] and (5). Theory is confronted with the experimental data in more detail in Table 3.

The second part of Fig. 5 shows the integrated leptoproduction cross section for the $2S$-state. The different node structure of the longitudinal and transverse wave functions leads to slightly different behaviour. In the longitudinal cross section there is a real zero at $Q^2 \cong 2.5$ GeV^2. In the transverse cross section both helicity parts of the wave function, cf. (11), contribute to the overlap with the photon. The relativistic component with $L_z = 1$ has its zero at a different transverse separation than the nonrelavistic part with $L_z = 0$ and aligned quark spins. Therefore the cross section has not a zero, but only a minimum at rather small $Q^2 \cong 0.3$ GeV^2 and a plateau at $Q^2 \cong 1$ GeV^2. The magnitude of the cross section decrases in both cases since the photon wave function shrinks in transverse extent at higher Q^2, and the inner negative parts of the excited vector meson wave functions become dominant. Asymptotically the longitudinal cross section dominates over the transverse by a power of Q^2; note, that for the $2S$-state we are not in the asymptotic region even at $Q^2 = 20$ GeV^2.

In Fig. 6 we show the ratio

$$R_{LT} = \sigma_L/\sigma_T \tag{21}$$

of longitudinal to transverse cross sections for the ρ- and $2S$-states including all Q^2 virtualties up to 20 GeV^2. For the ρ-meson the rapid rise of R_{LT} is confirmed quite well. We remark that an analysis of colour transparency in nuclei [26] should include a rapidly increasing ratio of longitudinal to transverse cross sections.

In Fig. 7 the respective differential cross sections are shown. For the $1S$-meson production the longitudinal and transverse differential cross sections follow roughly exponential behaviour with a slight upward curvature at larger $-t$ values. In comparison the $2S$-state produces sharp dips in the differential cross sections which occur at the same Q^2 where the integrated cross sections have minima. The occurence of the dips is a consequence of the node in the wave function, the exact location of these minima is highly parametrization dependent. At these Q^2-values where the minima occur the cross section is much faster falling off than in general. For an experiment where the superposition of longitudinal and transverse cross sections will be measured, these sharper fall-offs may be a good signal for interesting physics.

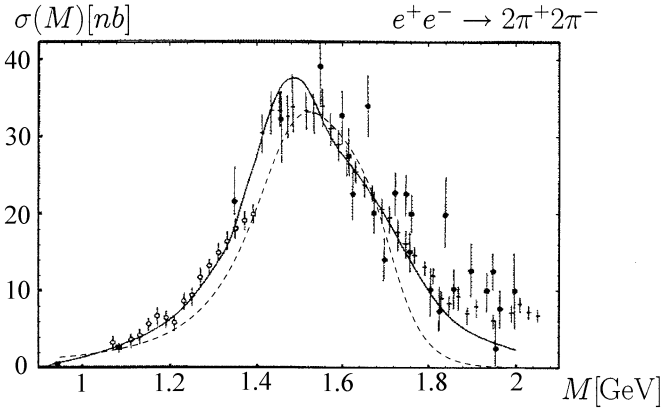

Fig. 8. Mass spectrum of e^+e^--annihilation into $2\pi^+2\pi^-$. The full line is a fit by Donnachie and Mirzaie [6]. The dashed line is the result of the parametrization used in this paper (see Table 2 and Appendix A)

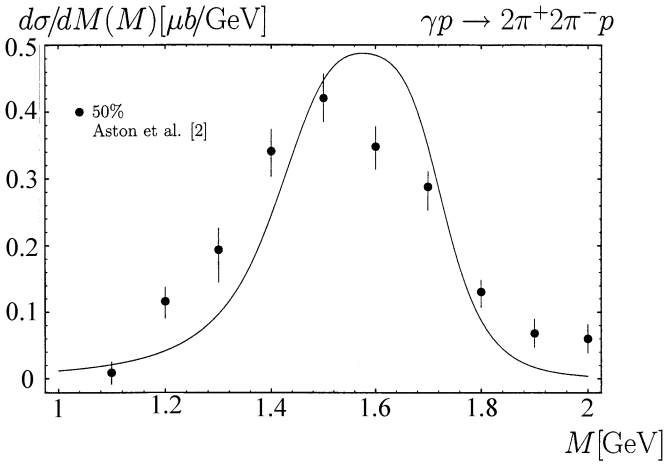

Fig. 9. Our result for the mass spectrum of photoproduced $2\pi^+2\pi^-$. The data are from [2], scaled with a factor 0.5

We revisit now the $\pi^+\pi^-$- and $2\pi^+2\pi^-$-production experiments across the $1-2$ GeV mass region. The most interesting result of the experiments is the different interference pattern in e^+e^--annihilation compared to photoproduction. In our convention the $2S$-wave function is negative relative to the ground state wave function at the origin so that the interference pattern determines the mixing angle to be in the first quadrant which gives opposite signs for the ρ'- and ρ''-annihilation amplitudes, i.e. the ρ-, ρ'- and ρ''-annihilation amplitudes have the relative signs $(+,-,+)$. In Fig. 1 the dashed curve shows the theoretical $\pi^+\pi^-$-mass distribution in e^+e^--annihilation according to the parametrization for ρ, ρ' and ρ'' used in this paper (see Table 2 and Appendix A). The data are from Orsay and Novosibirsk, Refs [4,5]; its main feature is the destructive interference slightly above 1.5 GeV which is correctly reproduced with the mixing angle $\theta = 41.2°$. Our parametrization also gives a sizeable $2\pi^+2\pi^-$-cross section of 40 nb in this range, see Fig. 8.

For photoproduction, however, cf. Fig. 2, experimental cross section from SLAC [1] show a small enhancement near the same energy. More recent data [27] even point to the possibility of $3S$-production. The different interference of the photoproduction amplitudes T_V, obeying the sign pattern $(+,+,-)$, comes from the dipole character of the cross section which favours the large-r part of the vector meson wave function more than the short range part which is important for the e^+e^--coupling. The theoretical $2\pi^+2\pi^-$-photoproduction cross section is shown in Fig. 9. It is experimentally very demanding to subtract the background in order to identify the resonating contribution.

Therefore it might be more realistic to look for the strong variation in the observables with Q^2 than for the absolute values. It should be noted that the strong variations of the cross sections with Q^2 in Figs. 5, 6 and 10 are a clear prediction of our model, the exact positions of the dips, however, depend crucially on the exact position of the node in the $2S$-state.

Experimentally also accessible is the ratio of $2\pi^+2\pi^-$-production via ρ' and ρ'' over $\pi^+\pi^-$-production via ρ:

$$R_\pi = \frac{\sigma^{f,T}_{(\rho'\rho'')} + \epsilon\sigma^{f,L}_{(\rho'\rho'')}\Big|_{f=2\pi^+2\pi^-}}{\sigma^{f',T}_{(\rho)} + \epsilon\sigma^{f',L}_{(\rho)}\Big|_{f'=\pi^+\pi^-}}\,, \tag{22}$$

where

$$\sigma^{f,\lambda}_{(\rho)} = \int_{s_f}^{\infty} dM^2 \frac{1}{16\pi s^2}\int dt \left| T^\lambda_\rho(s,t)\sqrt{\frac{M_\rho \Gamma^{tot}_\rho}{\pi}} \times \frac{c_{\rho f}}{M^2 - M^2_\rho + iM_\rho\Gamma^{tot}_\rho}\sqrt{B_{\rho\to f}}\right|^2,$$

$$\sigma^{f,\lambda}_{(\rho'\rho'')} = \int_{s_f}^{\infty} dM^2 \frac{1}{16\pi s^2}\int dt \left| \sum_{V=\rho',\rho''} T^\lambda_V(s,t)\sqrt{\frac{M_V \Gamma^{tot}_V}{\pi}} \times \frac{c_{Vf}}{M^2 - M^2_V + iM_V\Gamma^{tot}_V}\sqrt{B_{V\to f}}\right|^2. \tag{23}$$

The interference between the ρ' and ρ'' reduces the result compared to the zero-width approximation to $47 \pm 18\,\%$, where the uncertainty is due to the uncertainty in the widths of the resonances (see Table 2).

In Fig. 10 we show R_π for $\epsilon = 1$: After a small fluctuation near $Q^2 = 1$ GeV^2 it increases continuously. The structure at small Q^2 comes from the conspiracy of the longitudinal and transverse parts in the ratio; due to our lack of knowledge of the exact position of the nodes there may be only a continuous rise in R_π instead of a structured fluctuation. Especially the transverse cross section is very sensitive to the shape of the $2S$-state, since the large transverse photon extends well across the node. The longitudinal photon even at small Q^2 mainly tests the inner negative part of the state. At high Q^2 our calculation of R_π should truely reflect physics at work and indeed is in qualitative agreement with preliminary data from H1 [28] which still have large error bars.

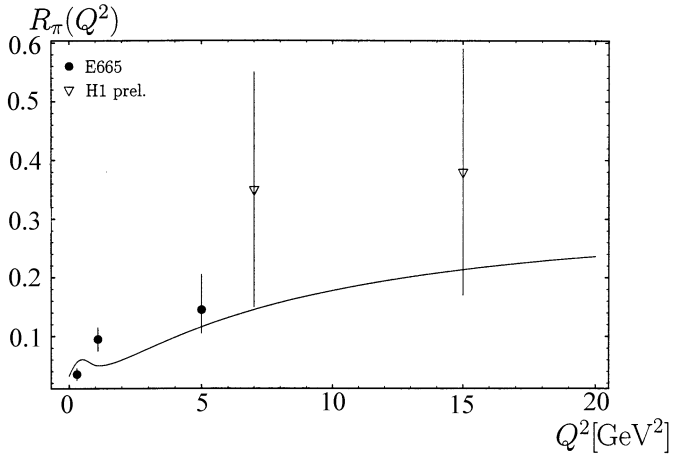

Fig. 10. Ratio R_π of $2\pi^+2\pi^-$-production via ρ' and ρ'' over $\pi^+\pi^-$-production via ρ as function of Q^2, cf. (22). Our curve is for to $\epsilon = 1$. Experimental points are taken from Refs [31] and [28]

4 Discussion and summary

In conclusion we have presented a realistic calculation for photoproduction which is based on a description of the ρ'- and ρ''-mesons as mixed quark-antiquark $2S$-states with some inert residual component. The decay characteristics of the ρ' point towards a sizeable hybrid admixture which may exist also for the ρ''. With our ansatz the different interference patterns in e^+e^--annihilation and photoproduction of two charged pions induce a mixing angle which implies that the ρ' and ρ'' are about one half a quark-antiquark $2S$-state and one half hybrid or $2D$-excitation. In this paper we give further evidence for the validity of the picture of diffraction as scattering of colour neutral states due to long-range gluon fluctuations. The large vector meson excited states test favourably our picture of a dipole-proton cross section increasing with the quark-antiquark transverse distance r due to string-string interactions which emerge from the model of the stochastic vacuum as a typical consequence of non-perturbative QCD. Especially transverse photoproduction has a matrix element where the elementary dipole-proton cross section is sampled between 1 and 2 fm. It is the dipole-proton cross section in that range which explains the markedly different interference patterns for e^+e^--annihilation and photoproduction. If it turns out that with increasing energy the excitation of the residual hybrid state becomes more important, we would see some indication for a perturbative gluonic component in the photon wave function which has matrix elements with the intrinsic glue in the hybrid. This would at the same time open up a window to the world of nonexotic hybrids and give us more insight into the importance of perturbative physics in diffraction. We have calculated all diffractive cross sections at $\sqrt{s} = 20$ GeV, but argued that the calculated ratios as σ_L/σ_T are also valid at higher energies. This is seen in the good agreement with HERA-data [28]. A big challenge remains to combine this picture of long range string-string interactions due to the stochastic vacuum with short range perturbative gluon fluctuations in order to understand the energy dependence of diffraction.

Acknowledgements. We thank Sandi Donnachie for many illuminating discussions during his stay in Heidelberg and E.L. Gubankova for participation in the early stage of the work.

A Leptonic decay, l^+l^--annihilation

Vector meson leptonic decay width and l^+l^--annihilation cross section into the final states $f = \pi^+\pi^-$ and $2\pi^+2\pi^-$ are determined by the same S-matrix element:

$$S = \langle l^-(p,s)\, l^+(p',s')\,|S|\,V(q,\lambda)\rangle\ , \tag{A1}$$

where p, p' and q are the momenta, s, s' and λ the spins and the helicity, respectively. With the T-matrix given through $S =: i(2\pi)^4\delta_4(p+p'-q)\,T$ we have

$$\begin{aligned} T &= -e\,\bar u_s(p)\gamma^\mu v_{s'}(p')\frac{g_{\mu\nu}}{(p+p')^2+i\varepsilon} \\ &\quad\times\langle 0\,|J^\nu_{em}(0)|\,V(q,\lambda)\rangle\ , \\ &= -e^2\bar u_s(p)\gamma^\mu v_{s'}(p')\,\frac{1}{s}\,f_V M_V\varepsilon_\mu(q,\lambda)\ ; \end{aligned} \tag{A2}$$

in the last line we have introduced the total energy squared $s = (p+p')^2$ and the coupling f_V of the vector meson to the electromagnetic current, which is defined through

$$\langle 0\,|J^\mu_{\rm em}(0)|\,V(q,\lambda)\rangle = e f_V M_V \varepsilon^\mu(q,\lambda)\ . \tag{A3}$$

Averaging over incoming spins s and s' and summation over outgoing helicities λ gives

$$\begin{aligned} \sum{}' |T|^2 &= -\frac{e^4}{3}\left(\frac{f_V M_V}{s}\right)^2 \\ &\quad\times\sum_{s,s'}\mathrm{tr}\left[\gamma^\mu u_s(p)\bar u_s(p)\gamma_\mu v_{s'}(p')\bar v_{s'}(p')\right]\ , \\ &= +\frac{4e^4}{3}\left(\frac{f_V M_V}{s}\right)^2 s\cdot\left(1+\tfrac{2m_l^2}{s}\right)\ , \end{aligned} \tag{A4}$$

where m_l is the lepton mass.

The decay rate of the vector meson in its rest frame is

$$\begin{aligned} d\Gamma &= \frac{1}{2M_V}\,(2\pi)^4\delta_4(p+p'-q)\frac{d^3\mathbf{p}}{(2\pi)^3 2p_{0+}} \\ &\quad\times\frac{d^3\mathbf{p}'}{(2\pi)^3 2p'_{0+}}\sum{}'|T|^2\ ; \end{aligned} \tag{A5}$$

phase space integration leads to

$$\Gamma_{V\to l^+l^-} = \frac{4\pi\alpha^2}{3}\frac{f_V^2}{M_V}\cdot\left(1+\tfrac{2m_l^2}{M_V^2}\right)\sqrt{1-\tfrac{4m_l^2}{M_V^2}}\ . \tag{A6}$$

The differential cross section to produce in l^+l^--annihilation a real vector meson V is

$$\begin{aligned} d\sigma &= \frac{1}{2w(s,m_l^2,m_l^2)}\,(2\pi)^4\delta_4(p+p'-q) \\ &\quad\times\frac{d^3\mathbf{q}}{(2\pi)^3 2q_{0+}}\sum{}'|T|^2\ , \end{aligned} \tag{A7}$$

where $w(x,y,z)$ is the Källen function; after phase space integration it writes

$$\sigma_{l^+l^-\to V} = \frac{4\pi e^4}{3}\left(\frac{f_V}{M_V}\right)^2 \delta(s-M_V^2) \cdot \frac{1+\frac{2m_l^2}{M_V^2}}{\sqrt{1-\frac{4m_l^2}{M_V^2}}} \,. \quad \text{(A8)}$$

For electrons the m_l-depending factors in (A6) and (A8) can be neglected.

To calculate the ρ-channel mass spectra of photoproduction and e^+e^--annihilation into two and four charged pions we distribute the ρ-, ρ'- and ρ''-mesons according to simple Breit-Wigner resonances:

$$T(M^2) := T \cdot \sqrt{\frac{M_V \Gamma_V^{tot}}{\pi}} \, \frac{c_{Vf}}{M^2 - M_V^2 + iM_V\Gamma_V^{tot}} \,, \quad \text{(A9)}$$

where T is the corresponding T-amplitude. The constraint for the constants c_{Vf} is that the integrated cross section is not altered:

$$\int_{s_f}^{\infty} dM^2 \, \left|T(M^2)\right|^2 = |T|^2 \,, \quad \text{(A10)}$$

where the threshold s_f is either $(2m_\pi)^2$ or $(4m_\pi)^2$ for the respective final state. The factor $|T|^2$ drops out and it follows

$$c_{Vf} = \left[\tfrac{1}{2} + \tfrac{1}{\pi}\arctan\tfrac{M_V^2 - s_f}{M_V}\right]^{-1/2} \,, \quad \text{(A11)}$$

which numerically implies values exceeding 1 up to seven percent.

We finally have

$$\sigma_{e^+e^-\to f}(M^2) = \frac{4\pi e^4}{3}\left|\sum_{V=\rho,\rho',\rho''} \frac{f_V}{M_V}\sqrt{\frac{M_V\Gamma_V^{tot}}{\pi}} \times \frac{c_{Vf}}{M^2 - M_V^2 + iM_V\Gamma_V^{tot}} \sqrt{B_{V\to f}}\right|^2 \quad \text{(A12)}$$

(for the branching ratios, widths and masses cf. Table 2). For annihilation into $f = \pi^+\pi^-$ we parametrize in (A12) the ρ-width Γ_ρ^{tot} by the polynomial

$$\Gamma_\rho^{tot}\left[1 + a_1\cdot\left(\tfrac{M^2}{M_\rho^2} - 1\right) + a_2\cdot\left(\tfrac{M^2}{M_\rho^2} - 1\right)^2\right] \quad \text{(A13)}$$

and adjust a_1, a_2 and $c_{\rho,\pi^+\pi^-}$ in order to reproduce the experimental spectrum.

B Wave functions

Construction

In previous work, see Appendix A in [8], we explicitely constructed the photon wave function in the frame of light-cone perturbation theory. For the probability amplitude for a photon with momentum $q = (q^+, q^- = -Q^2/2q^+, \mathbf{q} = \mathbf{0})$, virtuality Q and helicity λ to fluctuate into a $q\bar{q}$-pair one has to calculate the expression[B1]

$$\tilde{\psi}^{h,\bar{h}}_{\gamma(Q^2,\lambda)}(z,\mathbf{k}) = \sqrt{N_c} e_f \delta_{f\bar{f}} \frac{\sqrt{z\bar{z}}}{z\bar{z}Q^2 + m^2 + \mathbf{k}^2} \times \bar{u}(zq^+, \mathbf{k}, h)\, \varepsilon^\mu(q,\lambda)\gamma_\mu\, v(\bar{z}q^+, -\mathbf{k}, \bar{h}) \,, \quad \text{(B1)}$$

where the quark carries zq^+ longitudinal, $\mathbf{k}$ transverse momentum and helicity h (the antiquark accordingly $\bar{z}q^+$, $-\mathbf{k}$ and $\bar{h}$). With the polarization vectors $\varepsilon(q,0) = (q^+/Q, Q/2q^+, \mathbf{0})$ and $\varepsilon(q,\pm1) = -1/\sqrt{2}\,(0,0,1,\pm i)$ and the convention of light-cone components $q^\pm = (q^0 \pm q^3)/\sqrt{2}$, $g_{+-} = 1$, a lengthy but straightforward evaluation of (B1) gives

$$\tilde{\psi}^{h,\bar{h}}_{\gamma(Q^2,\lambda)}(z,\mathbf{k}) = \sqrt{N_c}\, e_f \delta_{f\bar{f}} \Big\{ -2z\bar{z}\,Q\,\delta_{h,-\bar{h}}\cdot\delta^0_\lambda + \sqrt{2}\big[\pm k\mathrm{e}^{\pm i\varphi_{\mathbf{k}}}\left(z\delta_{h+,\bar{h}-} - \bar{z}\delta_{h-,\bar{h}+}\right) + m\,\delta_{h\pm,\bar{h}\pm}\big]\cdot\delta^\pm_\lambda\Big\} \frac{1}{\varepsilon^2 + k^2} \,, \quad \text{(B2)}$$

where $k = |\mathbf{k}|$ and $\varepsilon = \sqrt{z\bar{z}Q^2 + m^2}$, cf. (4).

For an arbitrary function $\tilde{f}(\mathbf{k})$ we define the Fourier transform with respect to the transverse momentum $\mathbf{k}$ through

$$\int \frac{d^2\mathbf{k}}{(2\pi)^2}\, \mathrm{e}^{i\mathbf{k}\cdot\mathbf{r}}\, \tilde{f}(\mathbf{k}) = f(\mathbf{r}) \,. \quad \text{(B3)}$$

For an arbitrary function we have further:

$$\int \frac{d^2\mathbf{k}}{(2\pi)^2}\, \mathrm{e}^{i\mathbf{k}\cdot\mathbf{r}}\, k\mathrm{e}^{\pm i\varphi_{\mathbf{k}}}\, \tilde{f}(\mathbf{k}) = -i\left(\partial_1 \pm i\partial_2\right) f(\mathbf{r}) \,. \quad \text{(B4)}$$

If $\tilde{f}$ does not depend on the direction of $\mathbf{k}$, the r.h.s. of (B4) can be written as

$$-i\,\mathrm{e}^{\pm i\varphi_{\mathbf{r}}}\,\partial_r\, f(r) \,, \quad \text{(B5)}$$

where $r = |\mathbf{r}|$.

We thus have for the Fourier transform of (B2):

$$\psi^{h,\bar{h}}_{\gamma(Q^2,\lambda)}(z,\mathbf{r}) = \sqrt{N_c} e_f \delta_{f\bar{f}} \Big\{ -2z\bar{z}Q\,\delta_{h,-\bar{h}}\cdot\delta^0_\lambda + \sqrt{2}\big[\pm i\,\mathrm{e}^{\pm i\varphi_{\mathbf{r}}}\left(z\delta_{h+,\bar{h}-} - \bar{z}\delta_{h-,\bar{h}+}\right) \times(-\partial_r) + m\,\delta_{h\pm,\bar{h}\pm}\big]\cdot\delta^\pm_\lambda\Big\} \times \int \frac{d^2\mathbf{k}}{(2\pi)^2}\mathrm{e}^{i\mathbf{k}\cdot\mathbf{r}}\frac{1}{\varepsilon^2 + k^2} \,. \quad \text{(B6)}$$

With

$$\int \frac{d^2\mathbf{k}}{(2\pi)^2}\, \mathrm{e}^{i\mathbf{k}\cdot\mathbf{r}}\, \frac{1}{\varepsilon^2 + k^2} = \frac{K_0(\varepsilon r)}{2\pi} \quad \text{(B7)}$$

[B1] Throughout this appendix we abbreviate $\bar{z} = 1 - z$

and $-\frac{d}{dz}K_0(z) = K_1(z)$ (B6) becomes:

$$\begin{aligned}\psi^{h,\bar{h}}_{\gamma(Q^2,\lambda)}(z,\mathbf{r}) \qquad\qquad (B8)\\ = \sqrt{N_c}e_f\delta_{f\bar{f}}\Big\{ -2z\bar{z}Q\,\delta_{h,-\bar{h}}\,\frac{K_0(\varepsilon r)}{2\pi}\cdot\delta^0_\lambda\\ +\sqrt{2}\big[\pm i\varepsilon\,\mathrm{e}^{\pm i\varphi_\mathbf{r}}\left(z\delta_{h+,\bar{h}-}-\bar{z}\delta_{h-,\bar{h}+}\right)\\ \times\frac{K_1(\varepsilon r)}{2\pi}+m\,\delta_{h\pm,\bar{h}\pm}\,\frac{K_0(\varepsilon r)}{2\pi}\big]\cdot\delta^\pm_\lambda\Big\}\,,\end{aligned}$$

which is (2) and (3).

We model wave functions for the vector mesons according to the photon wave function:

$$\begin{aligned}\tilde{\psi}^{h,\bar{h}}_{V(\lambda)}(z,\mathbf{k}) = \Big\{4z\bar{z}\,\omega_{V,\lambda}\,\delta_{h,-\bar{h}}\cdot\delta^0_\lambda+\big[\pm k\mathrm{e}^{\pm i\varphi_\mathbf{k}}\\ \times\left(z\delta_{h+,\bar{h}-}-\bar{z}\delta_{h-,\bar{h}+}\right)+m\delta_{h\pm,\bar{h}\pm}\big]\cdot\delta^\pm_\lambda\Big\}\\ \times\tilde{\psi}_{V(\lambda)}(z,k)\,, \qquad (B9)\end{aligned}$$

where the energy denominator of the photon, $(z\bar{z}Q^2+m^2+\mathbf{k}^2)^{-1}$, has been replaced by functions $\tilde{\psi}_{V(\lambda)}(z,k)$ which also do not depend on the direction of $\mathbf{k}$. We define for the $1S$-state

$$\begin{aligned}\tilde{\psi}_{1(\lambda)}(z,k) &= \mathcal{N}_{1,\lambda}\sqrt{z\bar{z}}\,\mathrm{e}^{-\frac{1}{2}M^2\omega^{-2}_{1,\lambda}(z-1/2)^2}\cdot\frac{2\pi}{\omega^2_{1,\lambda}}\,\mathrm{e}^{-\frac{1}{2}\omega^{-2}_{1,\lambda}k^2},\\ &= h_{1,\lambda}(z)\cdot\frac{2\pi}{\omega^2_{1,\lambda}}\,\mathrm{e}^{-\frac{1}{2}\omega^{-2}_{1,\lambda}k^2} \qquad (B10)\end{aligned}$$

the harmonic oscillator parametrization by Wirbel and Stech, cf. [16], which is peaked at the nonrelativistic value $z = 1/2$. For the $2S$-state we have to differentiate that it can be "radially" excited either in longitudinal or, with two modes, in transverse direction. We thus introduce the simplest polynomial which is symmetric under exchange of $z \leftrightarrow \bar{z}$ in longitudinal direction and the transverse dependence of the $2S$-harmonic oscillator:

$$\begin{aligned}\tilde{\psi}_{2(\lambda)}(z,k) &= \mathcal{N}_{2,\lambda}\sqrt{z\bar{z}}\,\mathrm{e}^{-\frac{1}{2}M^2\omega^{-2}_{2,\lambda}(z-1/2)^2}\cdot\frac{2\pi}{\omega^2_{2,\lambda}}\,\mathrm{e}^{-\frac{1}{2}\omega^{-2}_{2,\lambda}k^2}\\ &\quad\times\big\{(z\bar{z}-A_\lambda)+\sqrt{2}\,(1-\omega^{-2}_{2,\lambda}k^2)\big\}\,,\\ &= h_{2,\lambda}(z)\cdot\frac{2\pi}{\omega^2_{2,\lambda}}\,\mathrm{e}^{-\frac{1}{2}\omega^{-2}_{2,\lambda}k^2}\\ &\quad\times\big\{(z\bar{z}-A_\lambda)+\sqrt{2}\,(1-\omega^{-2}_{2,\lambda}k^2)\big\}\,. \qquad (B11)\end{aligned}$$

In (B10) and (B11) we have used the definition of $h_{V,\lambda}(z)$ from (6), factors in which (B9) differs from (B2) are absorbed in the normalization constants $\mathcal{N}_{V,\lambda}$.

Fourier transformation of (B9) gives

$$\begin{aligned}\psi^{h,\bar{h}}_{V(\lambda)}(z,\mathbf{r}) = \Big\{4z\bar{z}\,\omega_{V,\lambda}\,\delta_{h,-\bar{h}}\cdot\delta^0_\lambda+\Big[\pm i\,\mathrm{e}^{\pm i\varphi_\mathbf{r}}\\ \times\left(z\delta_{h+,\bar{h}-}-\bar{z}\delta_{h-,\bar{h}+}\right)(-\partial_r)\\ +m\delta_{h\pm,\bar{h}\pm}\Big]\cdot\delta^\pm_\lambda\Big\}\,\psi_{V(\lambda)}(z,r)\,. \qquad (B12)\end{aligned}$$

Using

$$\int\frac{d^2\mathbf{k}}{(2\pi)^2}\,\mathrm{e}^{i\mathbf{k}\cdot\mathbf{r}}\cdot\frac{2\pi}{\omega^2_{1,\lambda}}\,\mathrm{e}^{-\frac{1}{2}\omega^{-2}_{1,\lambda}k^2} = \mathrm{e}^{-\frac{1}{2}\omega^2_{1,\lambda}r^2} \qquad (B13)$$

and

$$\begin{aligned}\int\frac{d^2\mathbf{k}}{(2\pi)^2}\mathrm{e}^{i\mathbf{k}\cdot\mathbf{r}}\cdot\frac{2\pi}{\omega^2_{1,\lambda}}\,\mathrm{e}^{-\frac{1}{2}\omega^{-2}_{1,\lambda}k^2}\,(1-\omega^{-2}_{1,\lambda}k^2)\\ = \mathrm{e}^{-\frac{1}{2}\omega^2_{1,\lambda}r^2}\,(\omega^2_{1,\lambda}r^2-1) \qquad (B14)\end{aligned}$$

we obtain the representations given in (8), (9) and (10), (11).

Fixing of the parameters

There are several parameters $\omega_{V,\lambda}$, $\mathcal{N}_{V,\lambda}$ and A_λ to be fixed. The constraints are as follows.

The first condition concerns the coupling to the electromagnetic current f_V, see (A3), which is connected with the wave function at the origin and determined by the vector meson e^+e^--decay width through

$$\Gamma_{V\to e^+e^-} = \frac{4\pi\alpha^2}{3}\frac{f_V^2}{M_V}\,; \qquad (B15)$$

cf. (A6) where the electron mass is neglected. With the wave functions given this means for $\lambda = L,\ \pm1$:

$$\begin{aligned}f_{V,L} &= \hat{e}_V\sqrt{N_c}\cdot4\,\omega_{V,L}\cdot\int\frac{dzd^2\mathbf{k}}{16\pi^3}\,4z\bar{z}\cdot\psi_{V(L)}(z,k)\,,\\ f_{V,T} &= \hat{e}_V\sqrt{N_c}\cdot\frac{4\sqrt{2}}{M_V}\cdot\int\frac{dzd^2\mathbf{k}}{16\pi^3}\left\{(z^2+\bar{z}^2)k^2+m^2\right\}\\ &\quad\times\frac{1}{4z\bar{z}}\cdot\tilde{\psi}_{V(\lambda=\pm1)}(z,k)\,, \qquad (B16)\end{aligned}$$

where $\hat{e}_V$ denotes the effective quark charge in the vector meson V in units of the electromagnetic charge, i.e. $\hat{e}_V = 1/\sqrt{2}$ for the ρ-mesons. Note, that in the transverse case the mass of the corresponding state enters explicitely; the numerical value of f_{2T} given in Table 1 is based on $M_{2S} = 1.6$ GeV.

The second condition is the normalization of the wave functions according to

$$\langle V(q',\lambda')|V(q,\lambda)\rangle = (2\pi)^3 2q^+\delta(q^+-q'^+)\delta_2(\mathbf{q}-\mathbf{q}')\delta_{\lambda\lambda'}\,, \qquad (B17)$$

i.e.

$$1 = \int\frac{dzd^2\mathbf{k}}{16\pi^3}\sum_{h,\bar{h}}\left|\tilde{\psi}^{h,\bar{h}}_{V(\lambda)}(z,\mathbf{k})\right|^2\,; \qquad (B18)$$

or explicitly for $\lambda = L,\ \pm1$:

$$\begin{aligned}1 &= 2\,\omega^2_{V,L}\cdot\int\frac{dzd^2\mathbf{k}}{16\pi^3}\,(4z\bar{z})^2\,\left|\tilde{\psi}_{V(L)}(z,k)\right|^2\,, \qquad (B19)\\ 1 &= 2\cdot\int\frac{dzd^2\mathbf{k}}{16\pi^3}\,\left\{(z^2+\bar{z}^2)k^2+m^2\right\}\,\left|\tilde{\psi}_{V(\lambda=\pm1)}(z,k)\right|^2\,.\end{aligned}$$

We first turn to the $1S$-state. Taken as input the experimentally well-determined quantities f_ρ and M_ρ, cf. Table 2, we have for each helicity the set of implicit equations (B16) and (B19) to determine $\omega_{1,\lambda}$ and $\mathcal{N}_{1,\lambda}$.

For the $2S$-state we exploit both the conditions of normalization, (B19), and orthogonality to the $1S$-state:

$$\begin{aligned} 0 &= \int \frac{dzd^2\mathbf{k}}{16\pi^3}(4z\bar{z})^2\ \tilde{\psi}^\dagger_{1(L)}(z,k)\tilde{\psi}_{2(L)}(z,k) \\ 0 &= \int \frac{dzd^2\mathbf{k}}{16\pi^3}\left\{(z^2+\bar{z}^2)k^2+m^2\right\} \\ &\quad\times\tilde{\psi}^\dagger_{1(\lambda=\pm1)}(z,k)\tilde{\psi}_{2(\lambda=\pm1)}(z,k)\ . \end{aligned} \tag{B20}$$

If one would set $\omega_{2,\lambda}=\omega_{1,\lambda}$ and determine $\mathcal{N}_{2,\lambda}$ and A_λ, the results for $f_{2,\lambda}$ from (B16) would not coincide for longitudinal and transverse polarization. However, it is possible to obtain agreement $f_{2L}=f_{2T}$, if one allows for slight deviation of ω_{2L} away from ω_{1L} and ω_{2T} away from ω_{1T}.

We refer to Table 1, where we list the numerical values of the so-determined parameters.

C Mixing angle, f_{2S}-coupling

We make some remarks on Table 2 and the derivation of the mixing angle θ from the branching ratios X_1, X_2 and X_3.

With our simple ansatz for the states $\rho(1450)$ and $\rho(1700)$ as mixtures of a quark-antiquark $2S$-state and an inert rest, cf. (1), we have

$$\begin{aligned} f_{\rho'} &= \cos\theta\ f_{2S}\ , \\ f_{\rho''} &= -\sin\theta\ f_{2S}\ . \end{aligned} \tag{C1}$$

For the leptonic decay widths, see (A6), this means

$$\begin{aligned} \Gamma_{\rho'\to e^+e^-} &= \frac{4\pi\alpha^2}{3}\ f_{2S}^2\ \frac{\cos^2\theta}{M_{\rho'}}\ , \\ \Gamma_{\rho''\to e^+e^-} &= \frac{4\pi\alpha^2}{3}\ f_{2S}^2\ \frac{\sin^2\theta}{M_{\rho''}}\ . \end{aligned} \tag{C2}$$

On the other side we have from (12)

$$\begin{aligned} \Gamma_{\rho'\to e^+e^-} &= \Gamma^{tot}_{\rho'}\cdot\left.\frac{X_1(1+X_2)}{X_3}\right|_{\rho'}\ , \\ \Gamma_{\rho''\to e^+e^-} &= \Gamma^{tot}_{\rho''}\cdot\left.\frac{X_1(1+X_2)}{X_3}\right|_{\rho''}\ . \end{aligned} \tag{C3}$$

Equating (C2) and (C3) we find

$$\begin{aligned} \tan^2\theta = {} & M_{\rho'}\Gamma^{tot}_{\rho'}\cdot\left.\frac{X_1(1+X_2)}{X_3}\right|_{\rho'}\Bigg/ M_{\rho''}\Gamma^{tot}_{\rho''} \\ & \cdot\left.\frac{X_1(1+X_2)}{X_3}\right|_{\rho''}\ . \end{aligned} \tag{C4}$$

and

$$\begin{aligned} f_{2S}^2 = \frac{3}{4\pi\alpha^2}\ \Bigg(& M_{\rho'}\Gamma^{tot}_{\rho'}\cdot\left.\frac{X_1(1+X_2)}{X_3}\right|_{\rho'} \\ & + M_{\rho''}\Gamma^{tot}_{\rho''}\cdot\left.\frac{X_1(1+X_2)}{X_3}\right|_{\rho''}\Bigg)\ , \end{aligned} \tag{C5}$$

i.e. numerically

$$\begin{aligned} \theta &= \ \ 41.2^\circ\ , \\ f_{2S} &= -0.178\ \text{GeV}\ , \end{aligned} \tag{C6}$$

where f_{2S} is negative and the mixing angle is chosen in the first quadrant to have the interference pattern in Fig. 1.

The coupling of the $2S$-state to the electromagnetic current apparently differs from the value in Table 1 which comes from our model $2S$-wave functions, cf. (10) and (11), which we require to be normalized and orthogonal on the $1S$-states. With regard to the accuracy of the numerical values of X_1, X_2 and X_3, cf. Table 2 and [6], we feel legitimized to base our calculation on the mixing angle derived above and the coupling in Table 1, instead of adjusting the wave function parameters in order to obtain global agreement.

References

1. D. Aston et al., Phys. Lett. B **92**, 215 (1980)
2. D. Aston et al., Nucl. Phys. B **189**, 15 (1981), and B **209**, 56 (1982)
3. A. Quenzer et al., Phys. Lett. B **76**, 512 (1978)
4. L.M. Barkov et al., Nucl. Phys. B **256**, 365 (1985)
5. D. Bisello et al., Orsay preprint, LAL: 85–15 (1985)
6. A. Donnachie, H. Mirzaie, Z. Phys. C **33**, 407 (1987)
7. A.B. Clegg, A. Donnachie, Z. Phys. C **62**, 455 (1994)
8. H.G. Dosch, T. Gousset, G. Kulzinger, H.J. Pirner, Phys. Rev. D **55**, 2602 (1997)
9. H.G. Dosch, T. Gousset, H.J. Pirner, Phys. Rev. D **57**, 1666 (1998)
10. J. Berges, D. Jungnickel, C. Wetterich, hep-ph/9705474
11. B.J. Schäfer, H.J. Pirner, hep-ph/9712413
12. F.E. Close, P.R. Page, Nucl. Phys. B **443**, 233 (1995) and Phys. Rev. D **56**, 1584 (1997)
13. L. Bergstrøm, H. Snellman, G. Tengstrand, Phys. Lett. B **80**, 242 (1979)
14. F. Cardelli, I.L. Grach, I.M. Narodetskii, G. Salme, S. Simula, Phys. Lett. B **349**, 393 (1995)
15. V.L. Morgunov, V.I. Shevchenko, Yu.A. Simonov, hep-ph/9704282
16. M. Wirbel, B. Stech, M. Bauer, Z. Phys. C **29**, 637 (1985)
17. I. Halperin, A. Zhitnitsky, Phys. Rev. D **56**, 184 (1997)
18. P. Ball, V.H. Braun, Phys. Rev. D **54**, 2182 (1996)
19. M. Diehl, hep-ph/9707441
20. H.G. Dosch, E. Ferreira, A. Krämer, Phys. Rev. D **50**, 1992 (1994)
21. B.Z. Kopeliovich, B.G. Zakharov, Phys. Rev. D **44**, 3466 (1991)
22. J. Nemcik, N.N. Nikolaev, E. Predazzi, B.G. Zahkarov, Phys. Lett. B **374**, 199 (1996); Z. Phys. C **75**, 71 (1997); J. Nemcik, N.N. Nikolaev, E. Predazzi, B.G. Zahkarov, V.R. Zoller, hep-ph/9712469

23. NMC-collaboration, M. Arneodo et al., Nucl. Phys. B **429** (1994) 503
24. E665-collaboration, M.R. Adams et al., MPI-PHE-97-03 Feb 1997, submitted to Z. Phys. C
25. A. Donnachie, P.V. Landshoff, Phys. Lett. B **296** (1992) 227
26. M.R. Adams et al., Phys. Rev. Lett. **74** (1994) 1525
27. P. Lebrun, E687-collaboration, Contribution to the 7th International Conference on Hadron Spectroscopy, Hadron 97, Aug 25–30, 1997 BNL, Upton NY, to appear in the proceedings
28. H1-collaboration, paper pa01-088, submitted to ICHEP 96, Warsaw 1996 (Poland)
29. M. Atkinson et al., Z. Phys. C **30** (1986) 531
30. Particle Data Group: Phys. Rev. D **54** (1996) 1
31. E665-collaboration, C. Salgado, CEBAF-workshop on colour transparency (1995)